Phase Transition Dynamics in One Dimensional Halide Perovskite Crystals

Minliang Lai[1], Teng Lei[1], Ye Zhang[1], Jianbo Jin[1], Julian A. Steele[1,2], Peidong Yang[1,3,4,5 *]

[1]Department of Chemistry, University of California, Berkeley, California 94720, USA.
[2]cMACS, Department of Microbial and Molecular Systems, KU Leuven, 3001 Leuven, Belgium
[3]Department of Materials Science and Engineering, University of California, Berkeley, CA 94720, USA.
[4]Materials Sciences Division, Lawrence Berkeley National Laboratory, Berkeley, CA 94720, USA.
[5]Kavli Energy NanoSciences Institute, Berkeley, California 94720, USA. California, 94720, USA.

[*]To whom correspondence should be addressed: p_yang@berkeley.edu (P.Y.)

ABSTRACT:

Triiodide perovskites $CsPbI_3$, $CsSnI_3$ and $FAPbI_3$ (where FA is formamidinium) are highly promising materials for a range of optoelectronic applications in energy conversion. However, they are thermodynamically unstable at room temperature, preferring to form low-temperature (low-T) non-perovskite phases with one dimensional (1D) anisotropic crystal structures. While such thermodynamic behavior represents a major obstacle toward realizing stable high-performance devices based on their high-temperature (high-T) perovskite phases, the underlying phase transition dynamics are still not well understood. Here we use *in situ* optical micro-spectroscopy to quantitatively study the transition from the low-T to high-T phases in individual $CsSnI_3$ and $FAPbI_3$ nanowires. We reveal a large blueshift in the PL peak (~38 meV) at the low-T /high-T two-phase interface of partially transitioned $FAPbI_3$ wire, which may result from the lattice distortion at the phase boundary. Compared to the experimentally derived activation energy of $CsSnI_3$ (~1.93 eV), the activation energy of $FAPbI_3$ is relatively small (~0.84 eV), indicating a lower kinetic energy barrier when transitioning from a face-sharing octahedral configuration to a corner-sharing one. Further, the phase propagation rate in $CsSnI_3$ is directly observed to be relatively high, which may be attributed to a high concentration of Sn vacancies. Our results not only facilitate a deeper understanding of phase transition dynamics in halide perovskites with anisotropic crystal structures but also enable controllable manipulation of optoelectronic properties *via* local phase engineering.

KEYWORDS:

Halide perovskites, phase transition, phase boundary, in-situ, $FAPbI_3$, $CsSnI_3$

Introduction

Controlling inherent phase transitions can allow for highly tunable optoelectronic properties when considering changes between significantly dissimilar semiconductor crystal lattices and structures[1,2]. Examination of such transition dynamics in semiconductors has not only facilitated a deeper understanding of complex electron–electron and electron-phonon interactions in correlated-electron materials[3], but also has led to novel functionalities, such as ultrafast switchable optoelectronics[4,5]. However, understanding the contributions of different symmetry and crystal structures to solid-solid phase transition dynamics and how defects can influence phase propagation remains limited.

As emergent semiconductor materials for optoelectronics[6–10], metal halide perovskites ABX_3 (A= Cs^+, $CH_3NH_3^+$, $NH_2CH{=}NH_2^+$, etc. B = Pb^{2+}, Sn^{2+}, etc. X = Cl^-, Br^-, I^-) are an ideal platform to study phase transition processes due to their rich structural phase transitions[11]. Their soft ionic lattices allow for a variety of transitions between low-temperature (low-T) non-perovskite and high-temperature (high-T) perovskite phases when the tolerance factor of the ionic radius deviates from the appropriate range to maintain a perovskite structure. For example, considering $CsPbBr_xI_{3-x}$ ($x \geq 2$) at room temperature, the relatively small ionic radius of atomic Cs^+ results in an edge-sharing BX_6 octahedral network, forming a 1D double-chain orthorhombic structure (Fig. 1a). Although $CsSnI_3$ and CsPbI3 share the same crystal structure, tin-based perovskites are dominated by Sn vacancy defects[12], owing to the presence of Sn^{4+}, rather than the halide vacancies which are commonly found in lead-based counterparts[13] (Fig. 1b). In formamidinium lead iodide ($FAPbI_3$), the PbI_6 octahedra are connected face-to-face to form 1D chains and a hexagonal crystal structure (Fig. 1c), because of the relatively large ionic radius of molecular cation $NH_2CH{=}NH_2^+$ (FA^+). Therefore, these materials are promising candidates for studying phase transition in 1D anisotropic crystals with different crystal structures (i.e. $CsPbI_3$ and $FAPbI_3$) and different defect types (i.e. $CsPbI_3$ and $CsSnI_3$). While many efforts have been made to preserve the high-T phases in these compositions and realize high-performance optoelectronic applications[14–18], their phase transition dynamics is still poorly understood. The dramatic change in optical properties between the high-T and low-T phases enable direct observation of the phase transition dynamics, via optical imaging and spectroscopy. Recently we systemically studied the phase transition nucleation and propagation in $CsPbBr_2I$ nanowires with an activation energy around 2.18 eV[19]. Here we observe

a relatively low activation energy (~0.84 eV) in $FAPbI_3$, indicating a small kinetic barrier when transforming from a face-sharing octahedral configuration to a corner-sharing one. In addition, the high Sn vacancy concentration is likely to facilitate the high phase propagation rate observed in $CsSnI_3$. Our results can promote the understanding of how crystal structures and defect types direct the phase transition in halide perovskites with 1D anisotropic crystal structures. Moreover, control over phase transition may provide potential solutions towards regulating the corresponding desired optoelectronic properties.

Results and discussion

The thermodynamically stable low-T phase $CsPbBr_xI_{3-x}$ and $CsSnI_3$ nanowires or microwires were directly synthesized via our previous reported methods[20,21]. Low-T phase $FAPbI_3$ microwires can be obtained via a similar solution processing method (Fig. S1, detail in SI). The wires present with a hexagonal cross-section (Fig. S2), reflecting its hexagonal crystal structure. Owing to the 1D anisotropy in these crystal structures (Fig. 1a-1c), the wire morphology of low-T phases can be successfully synthesized. These low-T phases undergo phase transition after thermal annealing and subsequent cooling in an inert atmosphere. *Ex-situ* powder x-ray diffraction (PXRD) in Fig 1d-e confirms that $CsPbBr_xI_{3-x}$ and $CsSnI_3$ transform from an edge-sharing non-perovskite orthorhombic phase to a corner-sharing orthorhombic perovskite structure. The PXRD shows the phase transition in $FAPbI_3$ to a corner-sharing perovskite cubic phase (Fig. 1f).

The low-T phases usually have a large bandgap energy and poor optical response/activity, i.e. exhibiting weak and broad photoluminescence (PL). The bandgap is dramatically reduced and the PL emission is significantly enhanced, accompanying with the formation of their high-T phases after thermal heating. Specifically, the strong and narrow PL emission peaks are shown in Fig. 1g-1i; $CsPbBr_2I$ features a narrow peak at ~580 nm, $CsSnI_3$ at ~ 950 nm, and $FAPbI_3$ ~820 nm. Thus, we aim to utilize this significant contrast in optical activity between the low- and high-T phases to monitor the phase transition dynamics. Previously we have reported an *in-situ* thermal induced phase transition study via SEM-cathodoluminescence (SEM-CL) based on this large difference in emission intensity[19]. Although *in-situ* SEM-CL experiments while heating provide high spatial resolution, the relatively harsh conditions required for these experiments – including high vacuum

and high-energy electron beam exposure may cause degradation and decomposition in the typically more vulnerable organic-inorganic perovskites, like $FAPbI_3$.

It follows that all-optical microscopy methods provide far more stable conditions, being non-contact and less destructive to the characterized materials. When heating under an inert atmosphere, the low- and high-T phases can be clearly differentiated *in situ* using the contrast created in their reflection of white light. Under white light illumination, the initial low-T phase $FAPbI_3$ wires appear relatively light, due to their large bandgap (~2.54 eV) and weak visible absorption. However, their appearance becomes much darker after a phase transition at high temperatures because of the large reduction in the bandgap (~1.53 eV), as depicted in Fig. S3. This suggests that the phase transition process and the two-phase interface propagation can be well-captured via all-optical imaging techniques. The different lattice vibrational signatures during the phase transition can further be resolved via Raman spectroscopy. We first confirm thermal phase evolution *in-situ* using Raman spectroscopy. As seen in Fig. 2A, below the phase transition temperature at 100 °C the low-T phase $FAPbI_3$ shows a strong peak at ~ 107 cm^{-1}, which corresponds to the Raman feature of δ-$FAPbI_3$ in previous reports[18,22]. At higher temperatures the low-T phase peak weakens and is replaced with a new band around 136 cm^{-1}, indicative of the formation of high-T perovskite phase at 140 °C. The coexistence of the two peaks at intermediate temperatures suggests the possible formation of a two-phase junction under the Raman micro-probe. The peak of low-T phase disappeared with a complete transition to the high-T phase when the temperature passed 150 °C.

Using a thermal quench to introduce a partial phase transition, we can obtain $FAPbI_3$ two-phase heterojunction for investigating the optical properties at the interphase boundary. Fig. 2b shows confocal PL spectra recorded from different locations in a two-phase heterojunction. The high-T phase segment of the wire is easily identified by its dark contrasting color, as shown in the corresponding optical image. The PL emissions measured at locations relatively far away from the interface (blue and green lines in Fig. 2b) peak around 820 nm, which is consistent with the emission of bulk High-T phase $FAPbI_3$. When approaching the interface (red line in Fig. 2b) the PL peak is seen to blueshift slightly (~7 meV) to 816 nm. Further, the blueshift is significantly enhanced (~38 meV) in the PL spectrum recorded at the two-phase interface (black line in Fig.

2b), peaking near 800 nm. The addition of periodic sub-peaks on the PL spectrum recorded at the junction may also indicate a strong exciton-phonon interaction. A large PL blue-shift (> 68 meV) was previously observed in α/δ phase junction $FAPbI_3$ thin film [23,24] and was attributed to the band bending of valence band and conduction band at the junction. However, we do not observe a noticeable blue-shift in a low-T/high-T phase $CsPbBr_xI_{3-x}$ nanowire (Fig. S4), indicating that the band offset of an intermediate band at the junction may not be the key reason in our phase heterojunctions. The different optical features in two-phase junctions of $FAPbI_3$ and $CsPbBr_xI_{3-x}$ most likely relate to their differences in microscopic structure at the phase boundary, which will be discussed in detail next.

The ex-situ selected area electron diffraction (SAED) from initial low-T phase and fully transformed high-T phase $FAPbI_3$ nanowires (Fig.3) can provide indirect evidence of the microscopic crystal structure at the interface. The SAED pattern of a low-T phase $FAPbI_3$ nanowire (Fig. 3a) indicates that the nanowires are single crystalline and their growth directions may be indexed to the [001] axis (along the face-sharing 1D chain direction) of the hexagonal structure in Fig. 1c. Such a preferred growth direction results directly from the anisotropic crystal structure. The thermally transformed high-T phase nanowire shows a (pseudo-)cubic perovskite SAED pattern with the corner-sharing octahedral oriented along the long wire axis (Fig. 3b). Therefore, the most likely interphase orientation is that face-sharing 1D chain direction of low-T phase $FAPbI_3$ adjoins the corner-sharing octahedra of the high-T phase $FAPbI_3$. This configuration is similar to our previous study in $CsPbBr_2I$ nanowires, where the molecular simulations reveal the formation of an atomically thin structurally disordered amorphous interfacial layer[19]. Given that organic cations ($CH_3NH_3^+$ and FA^+) have larger polarizability than the rigid Cs^+ cation [25], it is reasonable to consider a thicker and more flexible disordered two-phase interface in $FAPbI_3$. The interfacial strain can propagate along the wire and may induce the distortion and tilting of octahedra close to the phase boundary (Fig. 3c). Consequently, the lattice distortion would introduce an increased bandgap[26] and thus can explain the blue-shift PL at the interface. The relatively rigid lattice in $CsPbBr_xI_{3-x}$ makes the structural distortion with an atomically thin layer and thus difficult to be reflected via PL spectrum in Fig. S4. Further, the more deformable lattice in $FAPbI_3$ may result in a strong electron-phonon coupling at the interface. Therefore, we

hypothesized that the lattice distortion owing to the disordered amorphous interfacial layer probably attributes to the significant PL blue-shift in Fig. 2b.

We next quantitatively assess the phase boundary propagation via *in situ* optical imaging while heating the samples under an inert atmosphere. Fig. 3a shows a time series of optical dark-field images of evolution from $FAPbI_3$ low-T phase to high-T phase, highlighting the clear contrast change. Due to the limitation of optical diffraction using visible light, microwires are more easily distinguished during the phase transition, while wires with smaller diameters (i.e. nanowires) are difficult to recognize, due to the difference in optical contrast. We measure the phase propagation rates of individual microwires at temperature ranging from ~150 to ~175 °C (Fig.S5). The black triangles symbols in Fig. 4b show the distribution of $FAPbI_3$ phase propagation rates. Here we observe average propagation rates ranging from a few hundred nm/s to a few μm/s. Thermal dissipation should not be the major contributor to the propagation speed here. A pure thermal propagation rate is estimated more than 1000 μm/s in halide perovskites, which is orders of magnitude faster than the phase propagation we see (detail see SI). Note that the relatively fast phase propagation makes it difficult to measure the phase propagation rate before reaching constant temperature. Thus, the phase propagation rate is calculated using the average temperature during the increasing ramp. Through fitting of these data with an Arrhenius function, the propagation rate in $FAPbI_3$ as a function of temperature reveals an activation energy of 0.84 ± 0.25 eV. This value is comparable to the calculated activation barrier value of ~0.6 eV, which was previously reported by Chen *et al.*[27].

The temperature dependent phase propagation rate of $CsSnI_3$ can be obtained in a similar fashion (Fig. S6, red squares in Fig. 3b), yielding a rate (~3 μm/s around 163 °C)which is roughly three orders of magnitude higher than the values of derived for $CsPbBr_2I$ nanowires (~3 nm/s at 163 °C)from our previous work[19] (blue line in Fig. 3b). Notably, the activation energy of $CsSnI_3$ (1.93 ± 0.30 eV) is slightly lower than the values of $CsPbBr_2I$ (~2.18 eV). Since the low-T phase of both $CsSnI_3$ and $CsPbBr_2I$ share the same crystal structure, it is not surprising that a similar kinetic barrier is observed during the transformation from edge-sharing to corner-sharing metal halide octahedra. Considering the phase growth in $CsPbBr_2I$ is expected to be directed via ion diffusion mechanism[19], the higher phase propagation rate may likely be attributed to the relatively

high concentration of Sn vacancies in $CsSnI_3$ perovskite. The other related processes may involve possible lattice distortion, the contribution from intrinsic electron/hole carriers in the $CsSnI_3$ lattice. A significantly smaller activation energy is observed in $FAPbI_3$, indicating a small kinetic barrier height to transition from a face-sharing phase to a corner-sharing octahedra configuration. We suggest that a molecular simulation might help to better elucidate the details of this transition and underlying microscopic mechanisms, such as how Sn vacancies facilitate accelerated phase propagation and how the rotation /orientation of dynamic organic cation FA^+ at the interface. These values of activation energy from non-perovskite-to-perovskite phases are much higher than those phase transitions within ideal cubic perovskite and distorted perovskite phases in $MAPbI_3$ (< 0.25 eV)[28]. Unlike the martensitic-like transformation which only involves with rotation of metal halide octahedral or reorientation of molecular cations, constructive transformation in these 1D anisotropic perovskite crystal undergoes ionic bond breaking and reformation. In oxide perovskite $(Mg,Fe)SiO_3$, for example, an anisotropic post-perovskite phase where the octahedra form edge-sharing rutile-like columns is transformed from the perovskite phase under extremely high pressure and temperature inside the earth's lowermost mantle[29]. The molecular simulation reveals a high activation energy (~2.3 eV) at 120 GPa in the phase transition pathway[30]. The experimental observation of such phase transition dynamics remain quite challenging so far. The halide systems studied here with analogous crystal structures may be alternative approaches to experimentally investigate phase transition dynamics in oxide perovskite crystals of great interests.

Conclusion

The structural phase transitions to corner-sharing perovskite phases in 1D anisotropic crystal structures ($CsPbBr_xI_{3-x}$,$CsSnI_3$, $FAPbI_3$) can be investigated via in-situ heating optical imaging and Raman spectroscopy. Compared to $CsPbBr_xI_{3-x}$, the low activation energy in $FAPbI_3$ indicates a small kinetical barrier for the transition from face-sharing to corner-sharing octahedra configuration. In contrast, the inherently high Sn vacancy concentration is likely to facilitate the relatively high phase propagation rate observed in $CsSnI_3$. Together, these results not only provide important details of the correlation of crystal structure and defect type to phase transition dynamics, but also enable the interpretation of these phenomena within the wider perovskite material family.

Supplementary material

Detailed method for nanowires synthesis, structural and composition characterizations, optical measurements, discussion of thermal propagation rate, SEM images and SEM-EDS of $FAPbI_3$, confocal PL spectra of a low-T/high-T $CsPbBr_xI_{3-x}$ nanowire heterojunction, optical images of $CsSnI_3$ phase transition.

Acknowledgement

This work was supported by the U.S. Department of Energy, Office of Science, Office of Basic Energy Sciences, Materials Sciences and Engineering Division, under Contract No. DE-AC02-05-CH11231 within the Physical Chemistry of Inorganic Nanostructures Program (KC3103). TEM Work at the NCEM, Molecular Foundry were supported by the Office of Science, Office of Basic Energy Science, of the U.S. Department of Energy under Contract No DE-AC02-05CH11231. M.L., T.L., Y.Z. J.B. thank Suzhou Industrial Park for the fellowship support.

Reference:

1. Y. Li, K. A. N. Duerloo, K. Wauson, and E. J. Reed: Structural semiconductor-to-semimetal phase transition in two-dimensional materials induced by electrostatic gating. *Nat. Commun.* **7**, 1 (2016).
2. M. Wuttig and N. Yamada: Phase-change materials for rewriteable data storage. *Nat. Mater.* **6**(11), 824 (2007).
3. C. Kübler, H. Ehrke, R. Huber, R. Lopez, A. Halabica, R. F. Haglund, and A. Leitenstorfer: Coherent Structural Dynamics and Electronic Correlations during an Ultrafast Insulator-to-Metal Phase Transition in VO_2. *Phys. Rev. Lett.* **99**(11), 116401 (2007).
4. Q. Wang, E. T. F. Rogers, B. Gholipour, C. M. Wang, G. Yuan, J. Teng, and N. I. Zheludev: Optically reconfigurable metasurfaces and photonic devices based on phase change materials. *Nat. Photonics* **10**(1), 60 (2016).
5. M. Wuttig, H. Bhaskaran, and T. Taubner: Phase-change materials for non-volatile photonic applications. *Nat. Photonics* **11**(8), 465 (2017).
6. H. Cho, S. Jeong, M. Park, Y. Kim, C. Wolf, C. Lee, J. H. Heo, A. Sadhanala, N. Myoung, S. Yoo, S. H. Im, R. H. Friend, and T. Lee: Overcoming the electroluminescence efficiency

limitations of perovskite light-emitting diodes. *Science* **350**(6265), 1222 (2015).

7. J. Burschka, N. Pellet, S.-J. Moon, R. Humphry-Baker, P. Gao, M. K. Nazeeruddin, and M. Grätzel: Sequential deposition as a route to high-performance perovskite-sensitized solar cells. *Nature* **499**(7458), 316 (2013).
8. R. S. Sanchez, M. S. De La Fuente, I. Suarez, G. Muñoz-Matutano, J. P. Martinez-Pastor, and I. Mora-Sero: Tunable light emission by exciplex state formation between hybrid halide perovskite and core/shell quantum dots: Implications in advanced LEDs and photovoltaics. *Sci. Adv.* **2**(1) (2016).
9. J.-H. Im, I.-H. Jang, N. Pellet, M. Grätzel, and N.-G. Park: Growth of $CH_3NH_3PbI_3$ cuboids with controlled size for high-efficiency perovskite solar cells. *Nat. Nanotechnol.* **9**(11), 927 (2014).
10. G. E. Eperon, G. M. Paternò, R. J. Sutton, A. Zampetti, A. A. Haghighirad, F. Cacialli, and H. J. Snaith: Inorganic caesium lead iodide perovskite solar cells. *J. Mater. Chem. A* **3**(39), 19688 (2015).
11. C. C. Stoumpos and M. G. Kanatzidis: The Renaissance of Halide Perovskites and Their Evolution as Emerging Semiconductors. *Acc. Chem. Res.* **48**(10), 2791 (2015).
12. E. L. da Silva, J. M. Skelton, S. C. Parker, and A. Walsh: Phase stability and transformations in the halide perovskite $CsSnI_3$. *Phys. Rev. B* **91**(14), 144107 (2015).
13. C. Eames, J. M. Frost, P. R. F. Barnes, B. C. O'Regan, A. Walsh, and M. S. Islam: Ionic transport in hybrid lead iodide perovskite solar cells. *Nat. Commun.* **6**(May), 7497 (2015).
14. A. Swarnkar, A. R. Marshall, E. M. Sanehira, B. D. Chernomordik, D. T. Moore, J. A. Christians, T. Chakrabarti, and J. M. Luther: Quantum dot–induced phase stabilization of α-CsPbI3 perovskite for high-efficiency photovoltaics. *Science.* **354**(6308), 92 (2016).
15. A. G. Kontos, A. Kaltzoglou, E. Siranidi, D. Palles, G. K. Angeli, M. K. Arfanis, V. Psycharis, Y. S. Raptis, E. I. Kamitsos, P. N. Trikalitis, C. C. Stoumpos, M. G. Kanatzidis, and P. Falaras: Structural Stability, Vibrational Properties, and Photoluminescence in $CsSnI_3$ Perovskite upon the Addition of SnF_2. *Inorg. Chem.* **56**(1), 84 (2017).
16. K. P. Marshall, M. Walker, R. I. Walton, and R. A. Hatton: Enhanced stability and efficiency in hole-transport-layer-free $CsSnI_3$ perovskite photovoltaics. *Nat. Energy* **1**(12), 1 (2016).
17. L. Gu, D. Zhang, M. Kam, Q. Zhang, S. Poddar, Y. Fu, X. Mo, and Z. Fan: Significantly

improved black phase stability of $FAPbI_3$ nanowires via spatially confined vapor phase growth in nanoporous templates. *Nanoscale* **10**(32), 15164 (2018).

18. Y. Chen, Y. Lei, Y. Li, Y. Yu, J. Cai, M. H. Chiu, R. Rao, Y. Gu, C. Wang, W. Choi, H. Hu, C. Wang, Y. Li, J. Song, J. Zhang, B. Qi, M. Lin, Z. Zhang, A. E. Islam, B. Maruyama, S. Dayeh, L. J. Li, K. Yang, Y. H. Lo, and S. Xu: Strain engineering and epitaxial stabilization of halide perovskites. *Nature* **577**(7789), 209 (2020).
19. C. G. Bischak, M. Lai, D. Lu, Z. Fan, P. David, D. Dong, H. Chen, A. S. Etman, T. Lei, J. Sun, M. Grünwald, D. T. Limmer, P. Yang, and N. S. Ginsberg: Liquid-Like Interfaces Mediate Structural Phase Transitions in Lead Halide Perovskites. *Matter* (in press) (2020).
20. M. Lai, Q. Kong, C. G. Bischak, Y. Yu, L. Dou, S. W. Eaton, N. S. Ginsberg, and P. Yang: Structural, optical, and electrical properties of phase-controlled cesium lead iodide nanowires. *Nano Res.* **10**(4) (2017).
21. Q. Kong, W. Lee, M. Lai, C. G. Bischak, G. Gao, A. B. Wong, T. Lei, Y. Yu, L.-W. Wang, N. S. Ginsberg, and P. Yang: Phase-transition–induced p-n junction in single halide perovskite nanowire. *Proc. Natl. Acad. Sci. U. S. A.* **115**(36) (2018).
22. Q. Han, S. H. Bae, P. Sun, Y. T. Hsieh, Y. Yang, Y. S. Rim, H. Zhao, Q. Chen, W. Shi, G. Li, and Y. Yeng: Single Crystal Formamidinium Lead Iodide ($FAPbI_3$): Insight into the Structural, Optical, and Electrical Properties. *Adv. Mater.* **28**(11), 2253 (2016).
23. J. A. Steele, H. Yuan, C. Y. X. Tan, M. Keshavarz, C. Steuwe, M. B. J. Roeffaers, and J. Hofkens: Direct Laser Writing of δ- To α-Phase Transformation in Formamidinium Lead Iodide. *ACS Nano* **11**(8), 8072 (2017).
24. F. Ma, J. Li, W. Li, N. Lin, L. Wang, and J. Qiao: Stable α/δ phase junction of formamidinium lead iodide perovskites for enhanced near-infrared emission. *Chem. Sci.* **8**(1), 800 (2016).
25. C. G. Bischak, A. B. Wong, E. Lin, D. T. Limmer, P. Yang, and N. S. Ginsberg: Tunable Polaron Distortions Control the Extent of Halide Demixing in Lead Halide Perovskites. *J. Phys. Chem. Lett.* **9**(14), 3998 (2018).
26. A. Dobrovolsky, A. Merdasa, E. L. Unger, A. Yartsev, and I. G. Scheblykin: Defect-induced local variation of crystal phase transition temperature in metal-halide perovskites. *Nat. Commun.* **8**(1), 1 (2017).
27. T. Chen, B. J. Foley, C. Park, C. M. Brown, L. W. Harriger, J. Lee, J. Ruff, M. Yoon, J. J.

Choi, and S. H. Lee: Entropy-driven structural transition and kinetic trapping in formamidinium lead iodide perovskite. *Sci. Adv.* **2**(10), 1 (2016).

28. P. S. Whitfield, N. Herron, W. E. Guise, K. Page, Y. Q. Cheng, I. Milas, and M. K. Crawford: Structures, Phase Transitions and Tricritical Behavior of the Hybrid Perovskite Methyl Ammonium Lead Iodide. *Sci. Rep.* **6**(June), 1 (2016).
29. T. Tsuchiya, J. Tsuchiya, K. Umemoto, and R. M. Wentzcovitch: Phase transition in $MgSiO_3$ perovskite in the earth's lower mantle. *Earth Planet. Sci. Lett.* **224**(3–4), 241 (2004).
30. A. R. Oganov, R. Martoňák, A. Laio, P. Raiteri, and M. Parrinello: Anisotropy of earth's D″ layer and stacking faults in the $MgSiO_3$ post-perovskite phase. *Nature* **438**(7071), 1142 (2005).

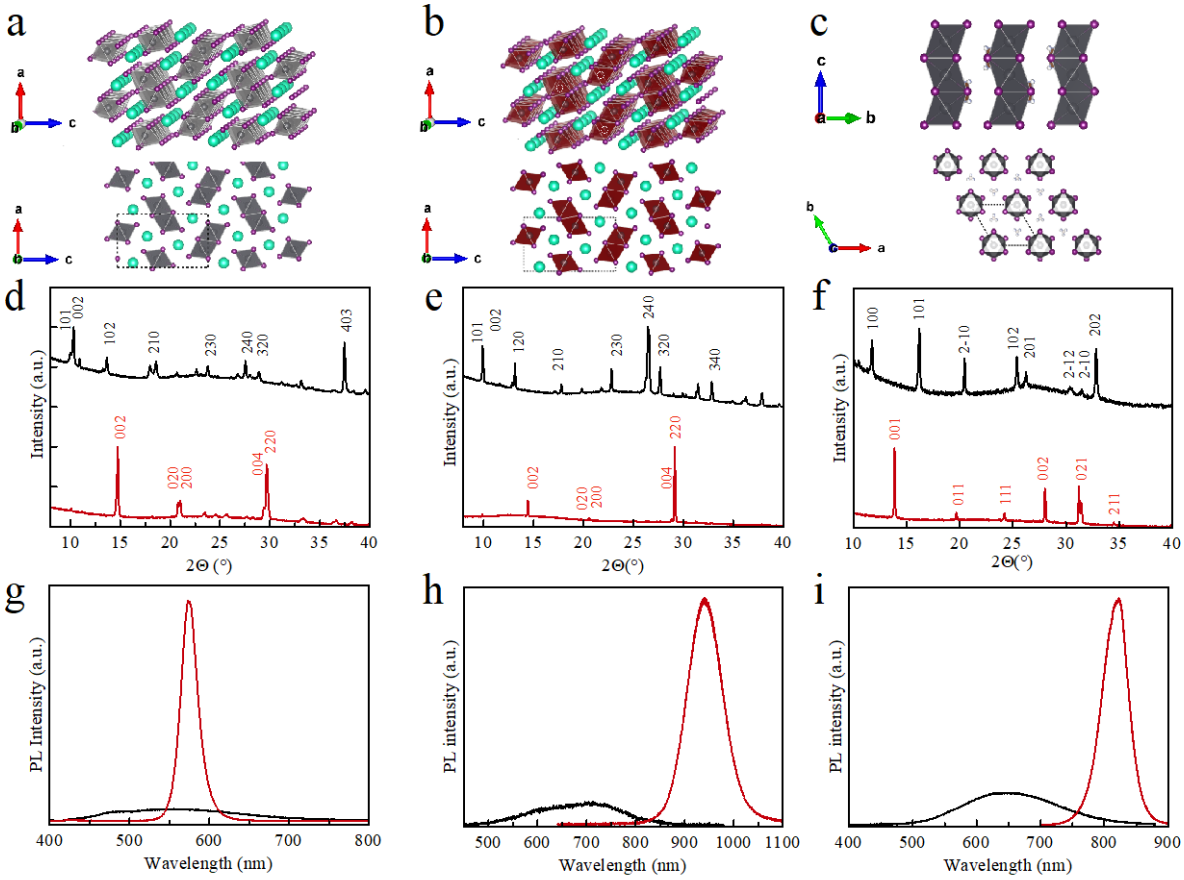

Figure 1. *Ex-situ* characterization of phase transition in 1D anisotropic halide perovskite. Schematic diagram of the structure of low-T phases of (**a**) $CsPbBr_xI_{3-x}$, (**b**) $CsSnI_3$, (**c**) $FAPbI_3$. (grey = Pb atoms; purple = X atoms; green = Cs atoms). Edge-sharing metal halide octahedral form 1D double-chain structure in orthorhombic $CsPbBr_xI_{3-x}$ and $CsSnI_3$. Sn vacancies are expected in $CsSnI_3$ due to the presence of Sn^{4+}. Face-sharing metal halide octahedral form 1D single-chain structure in hexagonal $FAPbI_3$. (**d-f**) PXRD patterns of as-synthesized low-T phases (black lines) and thermally transformed high-T phases (red lines) of $CsPbBr_2I$ (**d**) , $CsSnI_3$ (**e**), $FAPbI_3$(**f**). **(g-i)** PL intensity of as-synthesized low-T phases (black lines) and thermally transformed high-T phases (red lines) of $CsPbBr_2I$ (**g**) , $CsSnI_3$ (**h**), $FAPbI_3$ (**i**).

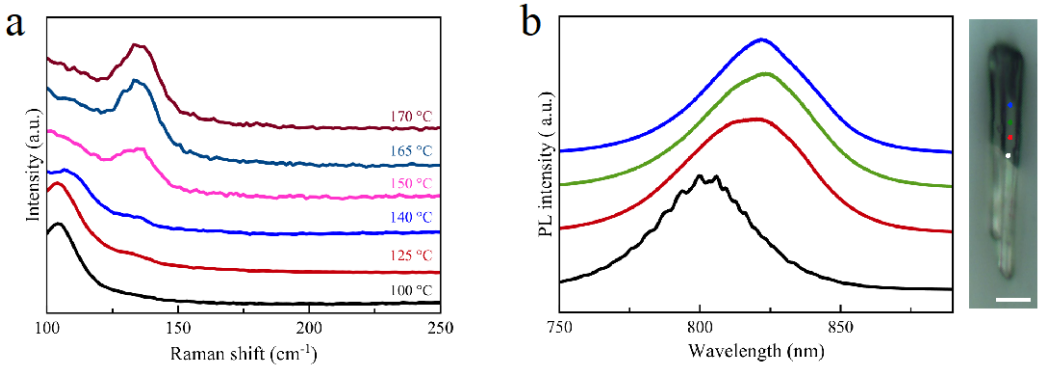

Figure 2. Optical measurements of $FAPbI_3$ phase transition. (**a**) *in-situ* Raman spectra evolution from low-T phase to high-T phase $FAPbI_3$. (**b**) Confocal PL spectra of a low-T/high-T two-phase heterojunction. The PL spectra of blue, green, red, black are corresponded to PL emission of the spots (blue, green, red, white) in the optical image. The scale bar is 5 μm.

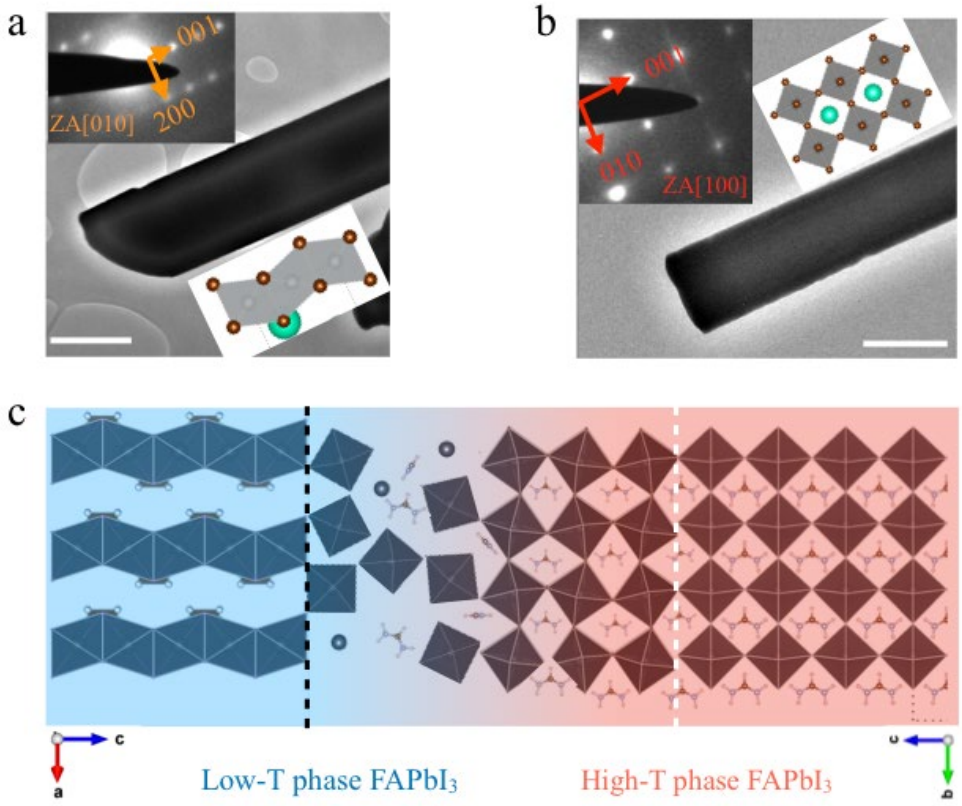

Figure 3. The TEM characterization of the low-T phase and high-T phase $FAPbI_3$. (**a**) The long axis direction in the low-T phase may be indexed to the [001] axis (along face-sharing 1D chain direction) of the hexagonal phase. (**b**)The thermal transformed high-T phase nanowire shows a cubic perovskite SAED pattern with the corner-sharing octahedral oriented along the long axis. The scale bar is 500 nm. (**c**) A proposed scheme of the crystal configuration at the phase interface. The face-sharing 1D chain direction of low-T phase abuts corner-sharing octahedral of high-T phase. A disordered amorphous interfacial layer exists at the phase boundary. The octahedral bonds are distorted and tilted close to the phase boundary.

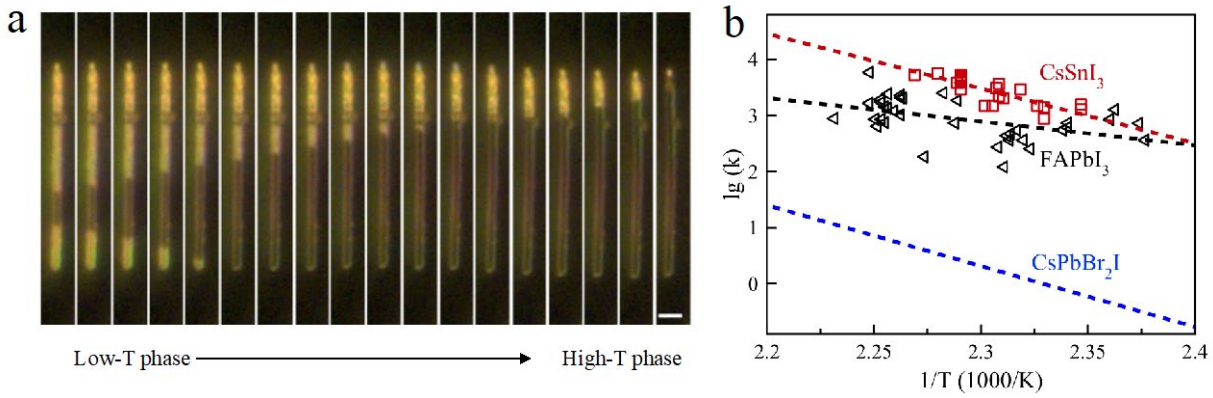

Figure 4. Optical imaging and quantitative analysis of perovskite phase propagation. (**a**) the time series of optical dark-field images of $FAPbI_3$ perovskite phase evolution. The temperature range is 155 -160 °C. Each frame is approximately 3s. The scale bar is 5 um. (**b**) propagation rate distribution and corresponding Arrhenius plot fitting. The vertical axis is $\log_{10}$ in nm/s units. The $FAPbI_3$ (black triangles) shows activation energy about 0.84 ± 0.25 eV. The $CsSnI_3$ (red squares) shows activation energy about 1.93 ± 0.30 eV. The blue line is the results of $CsPbBr_2I$ in ref 19.

TOC